Adiabatic Gradient Index Plasmonics

J. Valentine[1], T. Zentgraf[2], Y. Liu[2], M. Mikkelsen[2], X. Zhang[2]

[1]Department of Mechanical Engineering, Vanderbilt University
PMB 351592, 2301 Vanderbilt Place, Nashville, TN, USA
Fax: 1-615-343-6687; email: jason.g.valentine@vanderbilt.edu
[2]NSF Nanoscale Science and Engineering Center, University of California, Berkeley
3112 Etcheverry Hall, Berkeley, CA, USA
Fax: 1-510-643-2311; email (X. Zhang): xzhang@me.berkeley.edu

Abstract

We demonstrate an approach to realize gradient refractive index transformations in plasmonic systems by adiabatically tailoring the modal index. This is accomplished through smooth height variations in a dielectric cladding layer, thus minimizing parasitic scattering and reflections. We experimentally demonstrate this concept by examining plasmonic Luneburg and Eaton lenses.

1. Introduction

Recently, it has been proposed to apply transformation optics to plasmonic systems, aiming to manipulate the propagation of surface plasmon polaritons (SPPs) in a prescribed manner [1-3]. While the rigorous transformation optics approach requires spatial modulation of both the metal and dielectric, it was proposed that only transforming the dielectric medium is sufficient to mold the propagation of SPPs [1,2]. Furthermore, if a prudent transformation scheme is applied the transformed dielectric materials can be isotropic and non-magnetic [4]. In this case, the local effective index of SPPs is varied gradually and thus we term the approach gradient index (GRIN) plasmonics.

In this work, we demonstrate plasmonic Luneburg and Eaton lenses as a proof of principle of GRIN plasmonics [5]. Both lenses require a gradual change of the mode index which in general is difficult to obtain in traditional optical elements. The plasmonic Luneburg lens is similar to a traditional Luneburg lens in that it focuses SPPs to a point on the perimeter of the lens. The concept of the Luneburg lens was later generalized by Eaton for spherical lenses. Here, we use an Eaton lens formulation resulting in a 90° bend of an SPP [6]. We realize both GRIN SPP elements by spatially varying the height of a thin dielectric (ε = 2.19) Poly(methyl methacrylate) (PMMA) film on top of a gold surface.

2. Device Design and Realization

Changing the height of a dielectric cladding layer is a simple way to modify the SPPs effective index [1]. At a wavelength of 810 nm, the effective mode index of SPPs on a gold film can be changed from 1.02 to 1.54 as the height of the PMMA increases from zero to 500 nm (Fig. 1). Once the relationship between the SPP effective index and the PMMA height is known, the height profile for the Luneburg lens and Eaton lens can be readily interpolated to satisfy:

$$n = \sqrt{2-(r/R)^2} \qquad (1)$$

$$n^2 = \frac{R}{nr} + \sqrt{\left(\frac{R}{nr}\right)^2 - 1} \qquad (2)$$

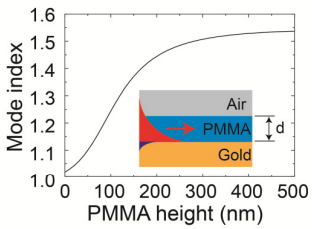

Fig. 1: Relationship between PMMA height and SPP index at 810 nm.

where (1) denotes the index variation for a Luneburg lens and (2) denotes the index variation for an

Eaton lens which bends light at 90°.

The experimental realization of the spatially varying PMMA height profile was achieved using grey-scale electron beam lithography (EBL). In this manner, the electron dose is continually varied across the sample in order to modulate the height of the PMMA layer and thus the mode index of SPPs. Fluorescence imaging and leakage radiation microscopy are applied to characterize the performance of the lenses.

3. Experimental Validation: Luneburg Lens

To validate the Luneburg lens performance using fluorescent imaging, infrared dye was incorporated into the PMMA and then spun and baked onto a 200-nm-thick Au film on top of quartz substrate. Grey-scale EBL exposure was then performed to realize the designed conical height profile as seen in Fig. 2(a) where an AFM trace across the centreline is shown in Fig. 2(d). Gratings were fabricated to launch the SPPs and were illuminated with 810 nm light. The fluorescence emitted from the dye (900 nm) was imaged on a silicon CCD camera. Fig. 2(b) shows a fluorescence image for SPPs passing the Luneburg lens. Since only the fluorescence was imaged the propagation of the SPPs is only visible at locations with PMMA on the gold surface, namely, in the conical PMMA structure region and behind the structure where the PMMA was not removed. As the SPPs enter the area of the lens (dotted circle) they are focused to the opposite circumference of the device as in a conventional Luneburg lens.

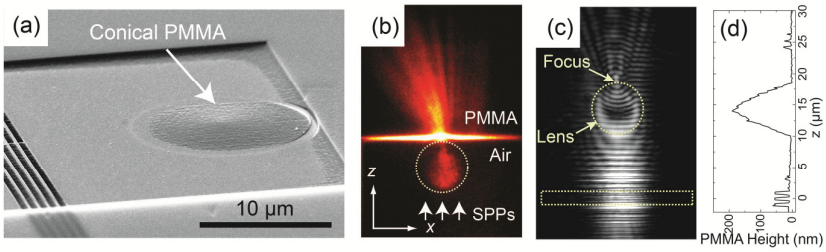

Fig. 2: (a) SEM image of fabricated Luneburg lens. (b) Experimentally measured fluorescence intensity profile of SPPs passing through the lens. (c) Leaky wave imaging of SPPs passing through the lens. (d) Height profile across the center-line of the lens.

To further validate the lens performance, leakage wave microscopy was utilized to better visualize SPP propagation both inside and outside of the lens. In this case, the Luneburg lens was fabricated on top of 50 nm Au to enable leakage of the SPPs through the substrate. The leakage radiation of the SPPs into the substrate was collected by an oil immersion objective and imaged to a silicon CCD camera. A typical image recorded for SPPs propagating through a Luneburg lens is shown in Fig. 2(c). The image exhibits the characteristic fringe pattern due to the interference of the directly transmitted light and the leakage radiation of the SPPs. Due to the coherence of the laser light, such interference fringes can give information about the phase evolution of the SPPs while propagating along the surface. As it can be seen from the image the phase front of the SPPs is flat when launched at the grating in the positive z direction. The SPP phase front starts curving inside the lens and leads to focusing at the circumference. After passing through the focal position of the lens the SPPs strongly diverge behind the lens and show the opposite phase front curvature.

3. Experimental Validation: Eaton Lens

Unlike the Luneburg lens, the refractive index of the Eaton lens quickly diverges as the center is approached. Since the PMMA coating can provide only a limited modal index range for SPPs from 1.02 up to 1.54 we are not able to realize the central part of the Eaton lens. For practical purposes we truncate the index profile at a maximum value of 1.54. A scanning electron microscopy image of the experimentally realized structure is shown in Fig. 3(a) together with the corresponding cross-section of the height profile, shown in Fig. 3(d). Although the profile is more complex than the Luneburg lens

ISBN 978-952-67611-0-7

the overall agreement is reasonably good; only the steepest part of the profile shows a small discrepancy from the theoretical model which is likely due to proximity effects during the exposure.

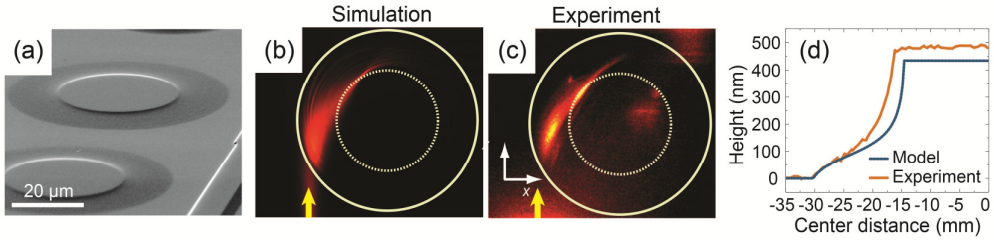

Fig. 3: (a) SEM image of the fabricated Luneburg lens (b) Simulation of SPP fluorescence intensity upon illumination of the lens. (c) Experimentally measured fluorescence intensity upon illumination of the device with SPPs. (d) Measured and theoretical height profile of the SPP Eaton lens.

A numerical simulation of the SPP propagation for the truncated Eaton lens is shown in Fig. 3(b). The excited SPPs are propagating in the positive z-direction and bend to the right side while passing through the lens. To extract the influence of the changing field magnitude we calculate the corresponding fluorescence intensity by taking the local thickness of the PMMA into account. Eventually SPPs leave the structure in the positive x-direction. Due to the inherent propagation loss of the SPPs the field magnitude decreases during the propagation. The truncation of the index in the center part of the lens leads to a small deviation from the perfect 90° bend. The SPP induced fluorescence emission intensity from the structure is shown in Fig. 3(c) in which the SPPs are propagating from the bottom in the positive z-direction and bend inside the Eaton lens to the right side.

4. Conclusion

In summary, we have experimentally demonstrated the feasibility of tailoring the propagation of SPPs by solely modifying the height of a dielectric cladding layer on top of a metal. Since the topology of the dielectric structure is slowly varied, this technique avoids optical losses associated with scattering and reflection from discrete structures. Our approach has the potential to achieve low-loss functional GRIN plasmonic elements and transformation optics inspired devices with a standard fabrication technology based on grey-scale electron beam lithography and is fully compatible with active plasmonics. The loss could be even further reduced by incorporating various gain materials into the dielectric material, leading to an increased propagation distance which is highly desired for all-optical devices or even plasmonic interconnects.

References

[1] Y. Liu, T. Zentgraf, G. Bartal, and X. Zhang, "Transformational plasmon optics.," *Optics Letters*, vol. 10, May. 2010, pp. 1991-1997.

[2] P.A. Huidobro, M.L. Nesterov, L. Martín-Moreno, and F.J. García-Vidal, "Transformation optics for plasmonics.," *Nano letters*, vol. 10, Jun. 2010, pp. 1985-1990.

[3] J. Renger, M. Kadic, G. Dupont, S.S. Aćimović, S. Guenneau, R. Quidant, and S. Enoch, "Hidden progress: broadband plasmonic invisibility," *Optics Express*, vol. 18, Jul. 2010, pp. 15757-15768.

[4] J. Li and J. Pendry, "Hiding under the Carpet: A New Strategy for Cloaking," *Physical Review Letters*, vol. 101, Nov. 2008, p. 203901.

[5] T. Zentgraf, Y. Liu, M.H. Mikkelsen, J. Valentine, and X. Zhang, "Plasmonic Luneburg and Eaton lenses.," *Nature Nanotechnology*, vol. 6, Jan. 2011, pp. 151-155.

[6] Aaron J. Danner, "Lossless Design of an Eaton Lens and Invisible Sphere by Transformation Optics with No Bandwidth Limitation - OSA Technical Digest (CD)," *Conference on Lasers and Electro-Optics/International Quantum Electronics Conference*, Optical Society of America, 2009, p. JThC4.

